Supplementary Information

High-Efficiency Blue Thermally Activated Delayed Fluorescence from Donor-Acceptor-Donor Systems *via* Through-Space Conjugation Effect

Feifei Gao‡, Ruiming Du‡, Chunmiao Han, Jing Zhang, Ying Wei, Guang Lu and Hui Xu*

Key Laboratory of Functional Inorganic Material Chemistry (Ministry of Education) & School of Chemistry and Material Science, Heilongjiang University, 74 Xuefu Road, Harbin 150080, P. R. China.

Content

Experimental Section

Materials and Instruments

All the reagents were purchased from Alfa. **4ArPBr2** (9,9'-(4,5-dibromo-1,2-phenylene)bis(9*H*-carbazole) and 9,9'-(4,5-dibromo-1,2-phenylene)bis(3,6-di-tert-butyl-9*H*-carbazole)) were synthesized according to our previous work[1].

^{1}H NMR spectra were recorded using a Varian Mercury plus 400NB spectrometer relative to tetramethylsilane (TMS) as internal standard. Molecular masses were determined by a MALDI-TOF-MS. Elemental analyses were performed on a Vario EL III elemental analyzer. The crystal suitable for single-crystal XRD analysis was obtained through slowly diffusing hexane into dichloromethane solution of **4CzDPDPO2A** at room temperature. All diffraction data were collected at 295 K on a Rigaku Xcalibur E diffractometer with graphite monochromatized Mo Kα (λ = 0.71073 Å) radiation in ω scan mode. All structures were solved by direct method and difference Fourier syntheses. Non-hydrogen atoms were refined by full-matrix least-squares techniques on F2 with anisotropic thermal parameters. The hydrogen atoms attached to carbons were placed in calculated positions with C−H = 0.93 Å and U(H) = 1.2Ueq(C) in the riding model approximation. All calculations were carried out with the SHELXL97 program. Thermogravimetric analysis (TGA) and differential scanning calorimetry (DSC) were performed on Shimadzu DSC-60A and DTG-60A thermal analyzers under nitrogen atmosphere at a heating rate of 10 °C min^{-1}. The morphological characteristics of the *vacuum*-evaporated films were measured with an atom force microscope (AFM) Agilent 5100 under the tapping mode. Cyclic voltammetric (CV) studies were conducted using an Eco Chemie B. V. AUTOLAB potentiostat in a typical three-electrode cell with a glassy carbon working electrode, a platinum wire counter electrode, and a silver/silver chloride (Ag/AgCl) reference electrode. All electrochemical experiments were carried out under a nitrogen atmosphere at room temperature in dichloromethane.

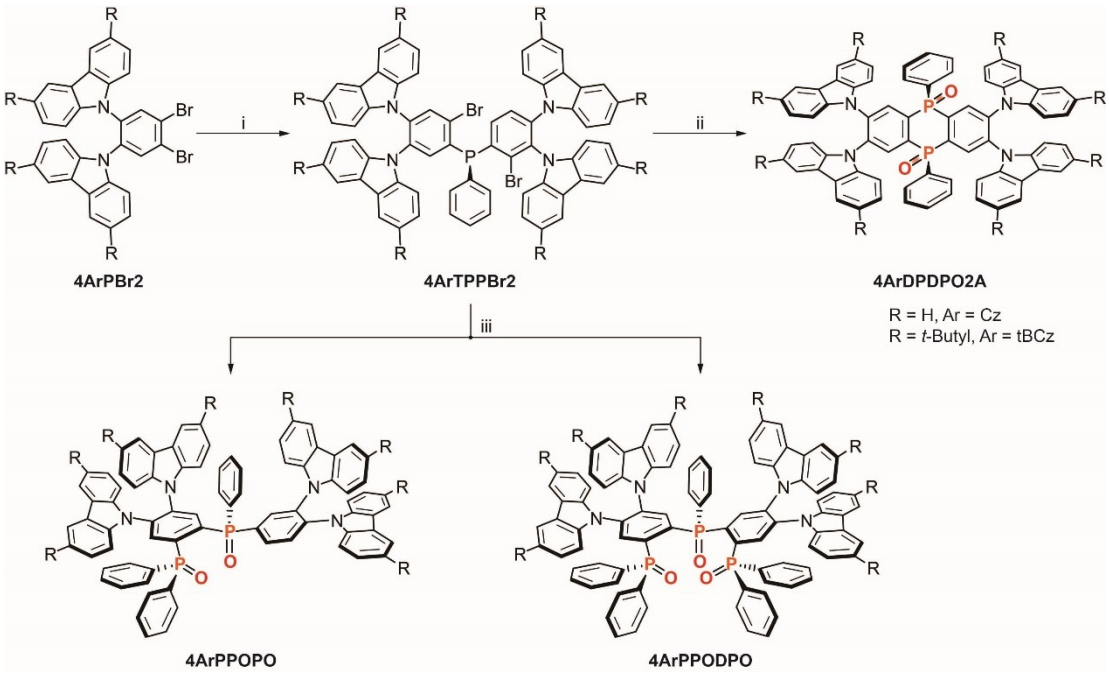

Scheme S1 Synthetic procedure of **4ArDPDPO2A, 4ArPPOPO and 4ArPPODPO**. i. *n*-BuLi, $PhPCl_2$, THF/ether, -120 °C to room temperature; ii. *n*-BuLi, $PhPCl_2$, THF, -78 °C to room temperature; 30% H_2O_2, CH_2Cl_2, room temperature; iii. *n*-BuLi, Ph_2PCl, THF, -78 °C to room temperature; 30% H_2O_2, CH_2Cl_2, room temperature.

Synthesis

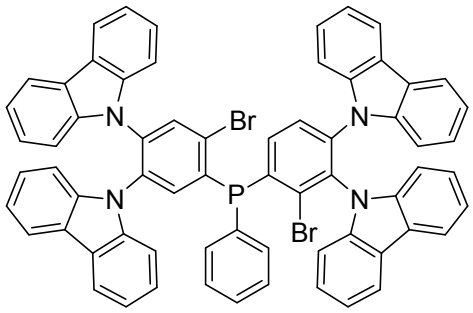

9,9',9'',9'''-((Phenylphosphanediyl)bis(5-bromobenzene-4,1,2-triyl))tetrakis(9H-carbazole) (**4CzTPPBr2**): 9,9'-(4,5-dibromo-1,2-phenylene)bis(9H-carbazole) (30.6 g, 54 mmol) was dissolved in anhydrous THF (400 ml) and Et_2O (400 ml). After cooling to -120 °C, *n*-BuLi (2.5 M in hexane, 21.6 ml, 54 mmol) was added in drops. The mixture was further stirred for 20 min at -120 °C. Then, $PhPCl_2$ (3.7mL, 27 mmol) was added to the mixture and stirred for another 20 min at -120 °C. The resulted gray solution was gradually warmed to room temperature and stirred

overnight. The reaction was quenched by addition of water. The mixture was treated with aqueous NH_4Cl (400 ml) and extracted with CH_2Cl_2 (3 × 400 ml). The organic phase was combined and dried over anhydrous Na_2SO_4. After removal of the solvent, the residue was chromatographed over silica gel using PE: DCM =3:2 as eluent to afford white solid with a yield of 20%. ^{1}HNMR (TMS, $CDCl_3$, 400 MHz): δ = 8.145 (d, J = 3.6 Hz, 2H), 7.745 (q, J_1 = 4.4 Hz, J_2 = 8.8 Hz, 4H), 7.683 (t, J = 7.2 Hz, 4H), 7.562 (t, J = 7.6 Hz, 2H), 7.421 (t, J = 7.6 Hz, 2H), 7.358 (d, J = 6.8 Hz, 2H), 6.839-7.110 ppm (m, 25H); ^{13}C NMR (TMS, $CDCl_3$, 100 MHz): δ = 138.066, 134.864, 134.688, 133.547, 133.177, 132.959, 132.590, 129.414, 128.583, 126.898, 124.573, 124.434, 122.572, 119.399, 108.321 ppm; LDI-TOF-MS (m/z, %): 1080 (100) [M^+]; elemental analysis (%) for $C_{66}H_{41}Br_2N_4P$: C 73.34, H 3.82, N 5.18; found: C 73.33, H 3.82, N 5.21.

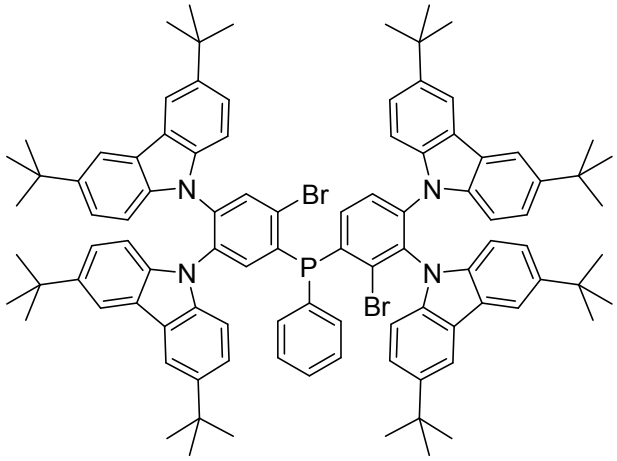

9,9',9'',9'''-((Phenylphosphanediyl)bis(5-bromobenzene-4,1,2-triyl))tetrakis(3,6-di-tert-butyl-9H-carbazole) (**4tBCzTPPBr2**): The synthetic procedure is similar to that of 9,9',9'',9'''-((phenylphosphanediyl)bis(5-bromobenzene -4,1,2-triyl))tetrakis(9H-carbazole), except for using 9,9'-(4,5-dibromo-1,2-phe nylene)bis(3,6-di-tert-butyl-9H-carbazole) (42.7 g, 54 mmol) instead of 9,9'-(4,5-dibromo-1,2-ph enylene)bis(9H-carbazole). The title compound was purified through flash column chromatography with silica gel and eluent as PE: DCM = 5:1 to afford white solid with a yield of 19%. ^{1}H NMR (TMS, CDCl3, 400 MHz): δ = 8.175 (d, J = 2.8Hz, 2H), 7.638 (t, J =8.0 Hz, 2H), 7.588 (s, 2H), 7.524-7.475 (m, 9H), 7.399-7.363 (m, 1H), 6.984 (d, J = 2.0 Hz, 1H), 6.962 (t, J =1.6 Hz, 1H), 6.901 (s, 1H), 6.879 (s, 1H), 6.779-6.670 (m, 8H),

6.531 (d, J = 2.4Hz, 2H), 6.509 (d, J = 2.4Hz, 2H), 1.331 (s, 18H),1.271 (s, 22H),1.252 (s, 16H), 1.223 ppm (s, 16H); ^{13}C NMR (TMS, $CDCl_3$, 100 MHz): δ = 142.023, 141.814, 141.697, 136.605, 136.349, 134.859, 133.442, 133.272, 133.056, 132.767, 132.599, 129.267, 128.549, 126.674, 126.344, 122.909, 122.599, 121.789, 114.107, 33.449, 30.841 ppm; LDI-TOF-MS (m/z, %): 1530 (100) [M^+]; elemental Analysis (%) for $C_{98}H_{105}Br_2N_4P$: C 76.95, H 6.92, N 3.66; found: C 76.97, H 6.93, N 3.70.

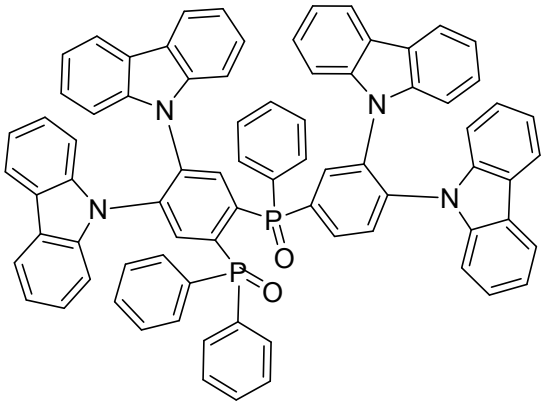

9,9'-(4-((4,5-Di(9H-carbazol-9-yl)-2-(diphenylphosphoryl)phenyl)(phenyl)phosphoryl)-1,2-phenylene)bis(9H-carbazole) (**4CzPPOPO**): **4CzTPPBr2** (1.1 g, 1 mmol) was dissolved in THF (10 ml). After cooling to -78 ^{o}C, 2.2 equivalents of n-BuLi (2.5 M in hexane) were added in dropwise. The mixture was further stirred for 1h at -78 ^{o}C. 1 equivalent of Ph_2PCl was added to the mixture, and the resultant gray solution was gradually warmed to room temperature and further stirred for 12 h. Then, 10 equivalents of 30% H_2O_2 was added in dropwise. After stirring for 1h, the reaction was quenched with water. The mixture was extracted with CH_2Cl_2 (3 × 10 ml), then the organic phase was combined and the solvent was removed in *vacuo*. The residue was purified with flash column chromatography over silica gel to afford the title compound as white crystals with a yield of 12%. ^{1}H NMR (TMS, $CDCl_3$, 400 MHz): δ = 8.853 (d, J = 13.2 Hz, 1H), 8.289 (d, J_1 = 12.8 Hz, 1H), 8.201 (t, J = 8.8 Hz, 1H), 8.034 (d, J = 13.2 Hz, 1H), 7.907 (t, J = 12.0 Hz, 3H), 7.712-7.773 (m, 8H), 7.405-7.573 (m, 11H), 7.286 (d, J = 10.4 Hz, 3H), 7.143-7.185 (m, 2H), 6.953-7.101 (m, 14H), 6.787-6.885 (m, 6H), 6.719 ppm (d, J = 8.0 Hz, 1H); ^{13}C NMR (TMS, $CDCl_3$, 100 MHz): δ = 138.375,

137.590, 137.491, 136.043, 134.074, 133.665, 132.581, 132.464, 131.925, 131.509, 131.322, 130.943, 122.710, 122.489, 122.302, 119.746, 119.053, 108.621 ppm; LDI-TOF-MS (m/z, %): 1138(100) [M^+]; elemental analysis (%) for $C_{78}H_{52}N_4O_2P_2$: C 82.23, H 4.60, N 4.92; found: C 82.25, H 4.62, N 4.95.

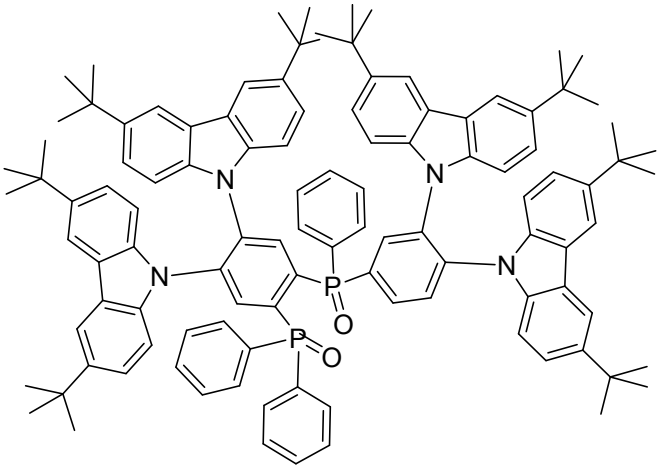

9,9'-(4-((4,5-Bis(3,6-di-tert-butyl-9H-carbazol-9-yl)-2-(diphenylphosphoryl)phenyl)(phenyl)phosphoryl)-1,2-phenylene)bis(3,6-di-tert-butyl-9H-carbazole) (**4tBCzPPOPO**): The procedure was similar to that of **4CzPPOPO**, except for using **4tBCzTPPBr2** instead of **4CzTPPBr2**, which afforded white powder with a yield of 13%. ^{1}H NMR (TMS, $CDCl_3$, 400 MHz) : δ = 8.767 (q, J_1 = 13.6Hz, J_2 = 3.6Hz, 1H), 8.273 (q, J_1 = 12.8Hz, J_2 = 1.6Hz, 1H), 8.195 (q, J_1 = 8.8Hz, J_2 = 4.0Hz, 1H), 7.108-7.156 (m, 1H), 7.381-7.359 (m, 3H), 7.692-7.358 (m, 20H), 7.308 (q, J_1 = 7.6Hz, J_2 = 2.8 Hz, 2H), 6.984-6.905 (m, 3H), 6.848-6.771 (m, 4H), 6.717-6.668 (m, 4H), 6.639-6.618 (m, 4H), 6.481(d, J = 8.8 Hz, 1H), 1.348-1.237 ppm (m, 72H); ^{13}C NMR (TMS, $CDCl_3$, 100 MHz): δ = 142.448, 141.643, 136.912, 136.546, 136.221, 136.011, 131.053, 127.398, 123.208, 122.962, 122.714, 122.534, 122.188, 122.064, 121.753, 114.417, 114.009, 107.954, 33.395, 30.783 ppm; LDI-TOF-MS (m/z, %): 1588 (100) [M^+]; elemental analysis (%) for $C_{110}H_{116}N_4O_2P_2$: C 83.19, H 7.36, N 3.53; found: C 83.18, H 7.35, N 3.56.

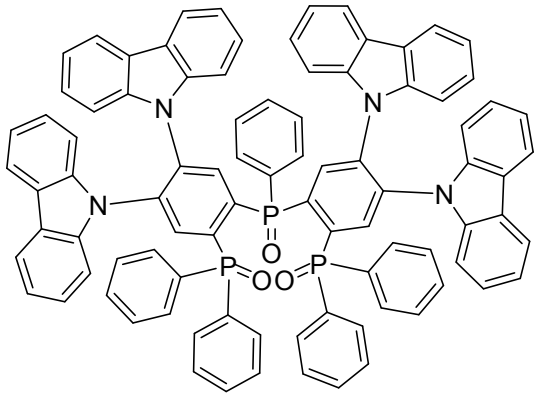

9,9'-(4-((4,5-Di(9H-carbazol-9-yl)-2,2'-bis(diphenylphosphoryl)phenyl)(phenyl)phosphoryl)-1,2-phenylene)bis(9H-carbazole) (**4CzPPODPO**): The procedure was similar to that of **4CzPPOPO**, except for using 2 equivalents of Ph_2PCl, which afforded white powder with a yield of 15%. ^1H NMR (TMS, $CDCl_3$, 400 MHz): δ = 8.707 (s, 2H), 8.01(s, 2H), 7.788 (d, J = 8.0 Hz, 6H), 7.679 (t, J = 6.8 Hz, 8H), 7.611 (t, J = 7.2 Hz, 3H), 7.412-7.704 (m, 18H), 7.089-7.137 (m, 6H), 7.033 (t, J = 7.2 Hz, 2H), 6.902-6.961 (m, 4H), 6.704-6.802 ppm (m, 10H); ^{13}C NMR (TMS, $CDCl_3$, 100 MHz): δ = 137.769, 135.128, 131.212, 130.776, 127.535, 126.772, 124.807, 124.435, 122.870, 122.338, 119.524, 118.935, 108.768 ppm; LDI-TOF-MS (m/z, %): 1338 (100) [M^+]; elemental analysis (%) for $C_{90}H_{61}N_4O_3P_3$: C 80.71, H 4.59, N 4.18; found: C 80.72, H 4.58, N 4.20.

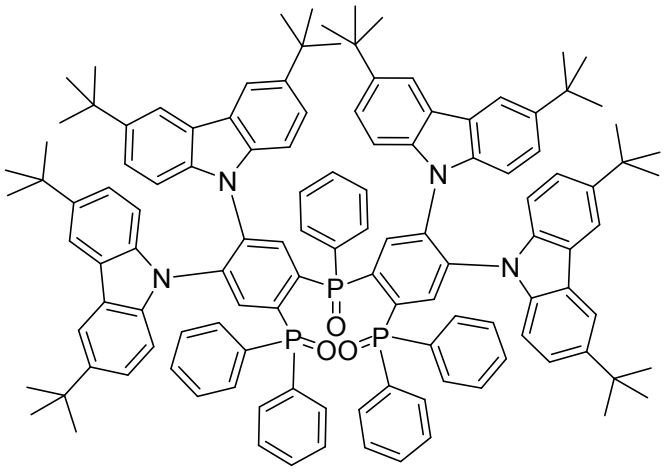

9,9'-(4-((4,5-Bis(3,6-di-tert-butyl-9H-carbazol-9-yl)-2,2'-bis(diphenylphosphoryl)phenyl)(phenyl)phosphoryl)-1,2-phenylene)bis(9H-carbazole) (**4tBCzPPODPO**): The procedure was similar to that of **4CzPPODPO**, except for using **4tBCzTPPBr2** instead of **4CzTPPBr2**, which afforded white powder with a

yield of 19%. ^{1}H NMR (TMS, $CDCl_3$, 400 MHz): δ = 8.557-8.477 (m, 2H), 8.898-8.819 (m, 2H), 7.661(q, J_1 = 11.6 Hz, J_2 = 7.2 Hz, 9H), 7.515(q, J_1 = 11.6 Hz, J_2 = 7.2 Hz, 13H), 7.406-7.360 (m, 11H), 6.823-6.710 (m, 12H), 6.477 (q, J_1 = 20.8Hz, J_2 = 8.8Hz, 4H), 1.308-1.224 ppm (m, 72H); ^{13}C NMR (TMS, $CDCl_3$, 100 MHz): δ = 142.015, 141.848, 136.397, 136.271, 131.471, 131.073, 130.462, 127.386, 122.895, 121.910, 121.781, 114.207, 108.025, 33.393, 30.794 ppm; LDI-TOF-MS (m/z, %): 1788(100) [M^+]; elemental analysis (%) for $C_{122}H_{125}N_4O_3P_3$: C 81.94, H 7.05, N 3.13; found: C 81.93, H 7.06, N 3.15.

General procedure of cyclization reaction: **4ArTPPBr2** (1 mmol) was dissolved in THF (10 ml). After cooling to -78 ^{o}C, 2.2 equivalents of n-BuLi (2.5 M in hexane) were added in dropwise. The mixture was further stirred for 1h at -78 ^{o}C. 1 equivalent of $PhPCl_2$ was added to the mixture, and the resultant gray solution was gradually warmed to room temperature and further stirred for 12 h. Then, 10 equivalents of 30% H_2O_2 was added in dropwise. After stirring for 1h, the reaction was quenched with water. The mixture was extracted with CH_2Cl_2 (3 × 10 ml), then the organic phase was combined and the solvent was removed in *vacuo*. The residue was purified with flash column chromatography over silica gel to afford the title compounds.

9,9',9'',9'''-(5,10-Diphenyl-5,10-dihydrophosphanthrene-2,3,7,8-tetrayl)tetrakis(9H-carbazole) oxides (**4CzDPDPO2A**): yellow crystals with a yield of 10%. ^{1}H NMR (TMS, $CDCl_3$, 400 MHz) : δ = 9.072 (t, J = 8.0 Hz, 4H), 7.823 (td, J_1 = 2.4 Hz, J_2 = 6.8 Hz, 8H), 7.378 (t, J = 7.2 Hz, 2H), 7.181-7.289 (m, 16 H), 7.064-7.142 ppm (m, 16 H); ^{13}C NMR (TMS, $CDCl_3$, 100 MHz): δ = 138.898, 135.002, 132.455, 130.838, 128.942, 126.270, 125.680, 124.352, 123.971, 121.089, 120.334, 109.753, 109.250 ppm; LDI-TOF-MS (m/z, %): 1060 (100) [M^+]; elemental analysis (%) for $C_{72}H_{46}N_4O_2P_2$: C 81.50, H 4.37, N 5.28; found: C 81.51, H 4.36, N 5.29.

9,9',9'',9'''-(5,10-Diphenyl-5,10-dihydrophosphanthrene-2,3,7,8-tetrayl)tetrakis(3,6-di-tert-butyl-9H-carbazole) oxides (**4tBCzDPDPO2A**): yellow powder with a yield of 14%. ^{1}H NMR (TMS, $CDCl_3$, 400 MHz) : δ =

8.461 (t, J = 8.0 Hz, 4H), 8.228-8.190 (m, 4H), 7.685 (s, 6H), 7.575 (d, J = 12 Hz, 8H), 6.842-6.818 (m, 8H), 6.788(d, J = 8.8Hz, 4H), 6.575(d, J = 8.8 Hz, 4H), 1.315 ppm (d, J = 4.0 Hz, 72H); ^{13}C NMR (TMS, $CDCl_3$, 100 MHz): δ = 142.543, 136.053, 133.557, 131.052, 128.377, 123.200, 122.852, 122.088, 121.796, 114.529, 114.322, 107.987, 107.416, 33.459, 30.783 ppm; LDI-TOF-MS (m/z, %): 1510 (100) [M^+]; elemental analysis (%) for $C_{104}H_{110}N_4O_2P_2$: C 82.72, H 7.34, N 3.71; found: C 82.73, H 7.35, N 3.73.

The cif and structure factor data are available from Cambridge structure database, CCDC number 1869741 (**4CzDPDPO2A**).

Photophysical Measurement

Absorption spectra of the target compound were measured using a SHIMADZU UV-3150 spectrophotometer spectrophotometer. Emission spectra were measured with an Edinburgh FPLS 920 fluorescence spectrophotometer. Phosphorescence spectra were recorded with a delay of 300 μs using Time-Correlated Single Photon Counting (TCSPC) method with a microsecond pulsed Xenon light source for 0.1 μs-10 s lifetime measurement, the synchronization photomultiplier for signal collection and the Multi-Channel Scaling Mode of the PCS900 fast counter PC plug-in card for data processing. The TADF dye doped films (100 nm) were prepared through vacuum evaporation for optical analysis and AFM measurement. Photoluminescence quantum yields (PLQY, η) of these films were measured through a labsphere 1-M-2 (ϕ = 6") integrating sphere coated by Benflect with efficient light reflection in a wide range of 200-1600 nm, which was integrated with FPLS 920. The absolute PLQY determination of the sample was performed by two spectral (emission) scans, with the emission monochromator scanning over the Rayleigh scattered light from the sample and from a blank substrate. The first spectrum recorded the scattered light and the emission of the sample, and the second spectrum contained the scattered light of Benflect coating. The integration and subtraction of the scattered light parts in these two spectra arrived at the photon number absorbed by the samples (N_a); while, integration of the emission of the samples to calculate the emissive photon number (N_e). Then, the absolute η can be estimated according to the equation of $\eta = N_e/N_a$.

Spectral correction (emission arm) was applied to the raw data after background subtraction, and from these spectrally corrected curves the quantum yield was calculated using aF900 software wizard.

DFT Calculations

DFT computations were carried out with different parameters for structure optimizations and vibration analyses. The ground state configuration of **4CzDPDPO2A** was established according to single crystal data. The ground, singlet and triplet states in vacuum were optimized by the restricted and unrestricted formalism of Beck's three-parameter hybrid exchange functional[2] and Lee, and Yang and Parr correlation functional[3] B3LYP/6-31G(d,p), respectively. The fully optimized stationary points were further characterized by harmonic vibrational frequency analysis to ensure that real local minima had been found without imaginary vibrational frequency. The total energies were also corrected by zero-point energy both for the ground state and triplet state. Natural transition orbital (NTO) analysis was performed on the basis of optimized ground-state geometries at the level of ωB97XD/6-31G(d,p).[4] The contours were visualized with Gaussview 5.0. All computations were performed using the Gaussian 09 package.[5]

Molecular Design

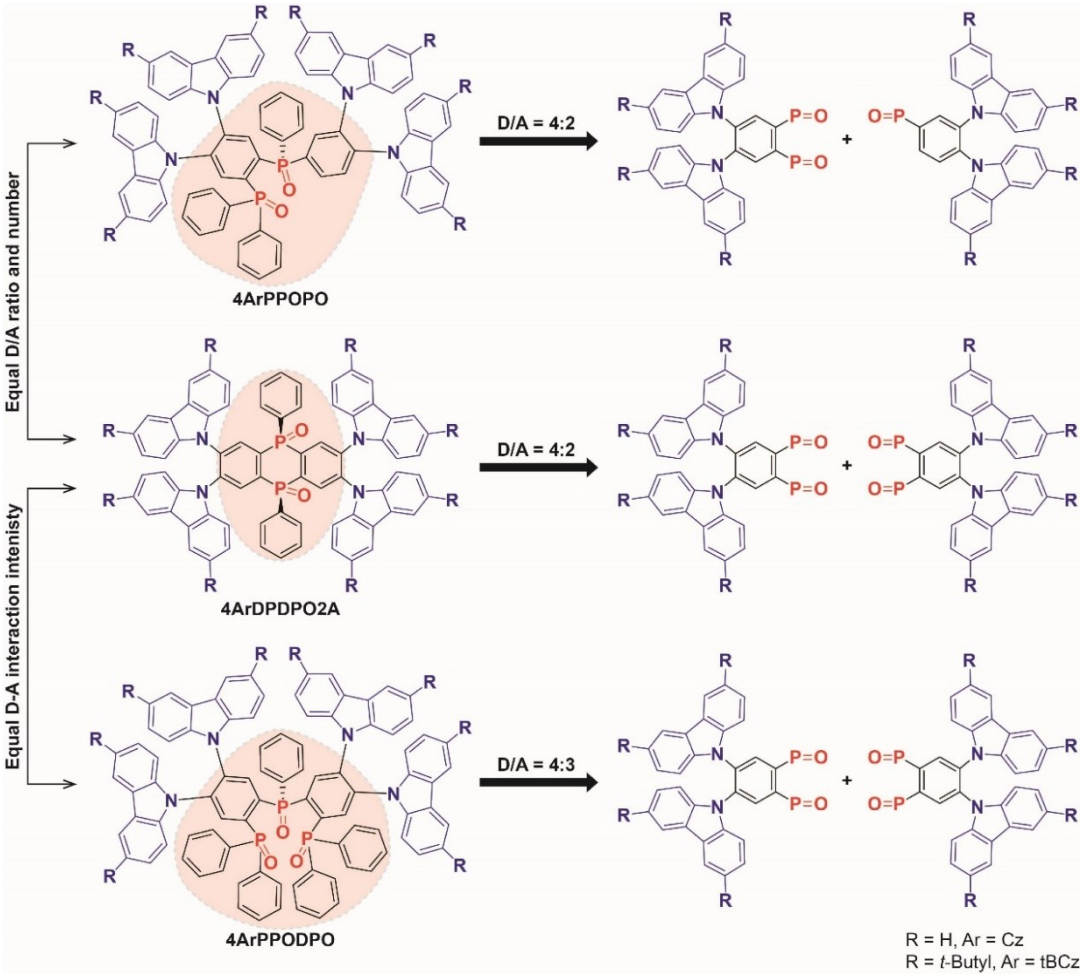

Scheme S2. Molecular design of 4ArDPDPO2A, 4ArPPOPO and 4ArPPODPO. The acceptor moieties were marked with red background color.

The phosphine oxide (PO) moieties in these molecules are the integral acceptors, namely DPDPO2A in **4ArDPDPO2A** and the central triphenylphosphine oxide with one or two DPPO substituents in **4ArPPOPO** and **4ArPPODPO**, respectively. The basic structures of **4ArDPDPO2A**, **4ArPPOPO** and **4ArPPODPO** are the same as four donors-bonded PO acceptors. The D (carbazole derivatives)/A (P=O groups) ratios in **4ArPPOPO** and **4ArDPDPO2A** are the same. Considering two of four D groups in **4ArPPOPO** have the D-A interaction with only one P=O group, **4ArPPODPO** were further prepared, in which each D group interacts with two P=O groups. Therefore, the D-A interaction intensities in **4ArPPODPO** and **4ArDPDPO2A** are the same. In this case, if only considering the number, ratio or interaction mode, the ICT interactions in **4ArPPOPO** and **4ArPPODPO** should be similar to that in

4ArDPDPO2A. The main reason resulting in the enhanced ICT effect in **4ArDPDPO2A** is their homoconjugated structures, in contrast to the insulting structures of **4ArPPOPO** and **4ArPPODPO**.

Molecular Packing of 4CzDPDPO2A by Single-Crystal X-Ray Diffraction

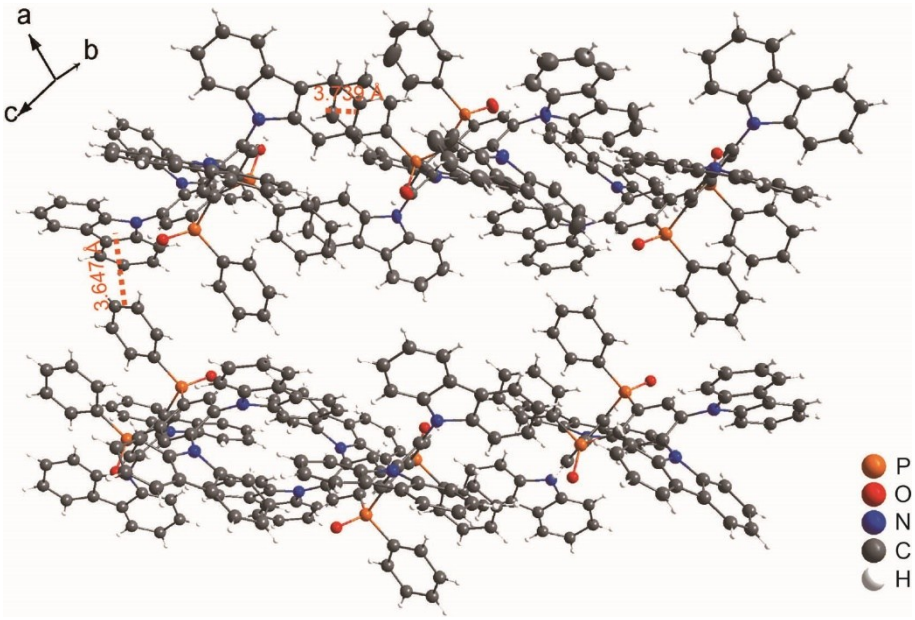

Figure S1. Single-crystal packing diagram of **4CzDPDPO2A**.

DFT Simulation Results

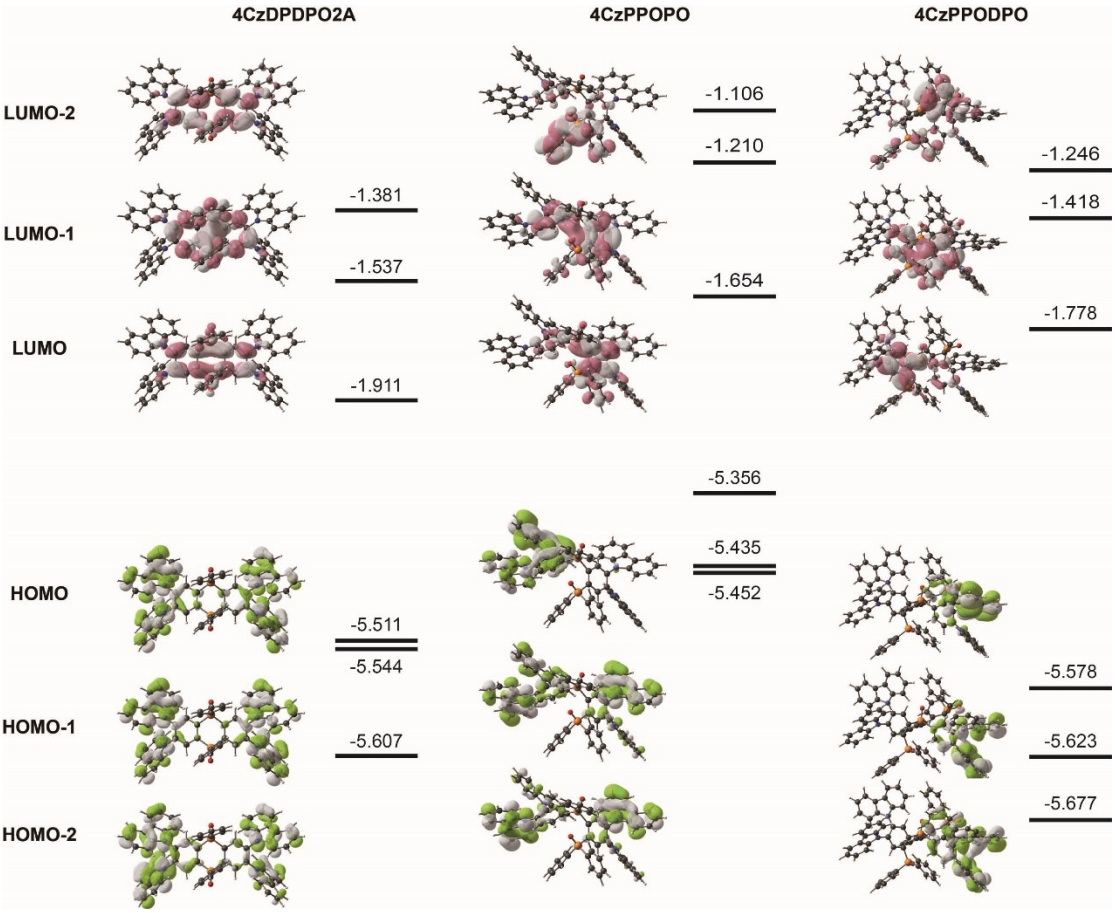

Figure S2. Contours and energy levels of the frontier molecular orbitals for **4CzDPDPO2A**, **4CzPPOPO** and **4CzPPODPO**.

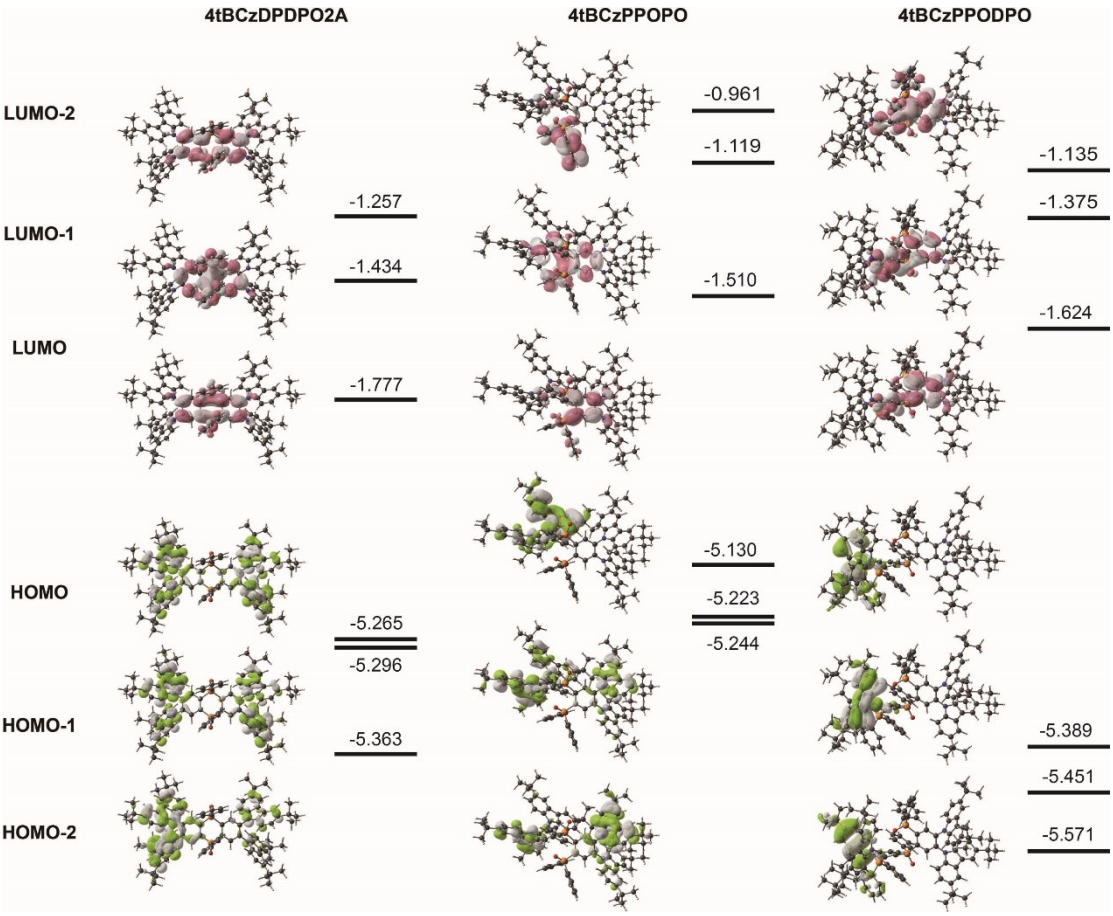

Figure S3. Contours and energy levels of the frontier molecular orbitals for **4tBCzDPDPO2A**, **4tBCzPPOPO** and **4tBCzPPODPO**.

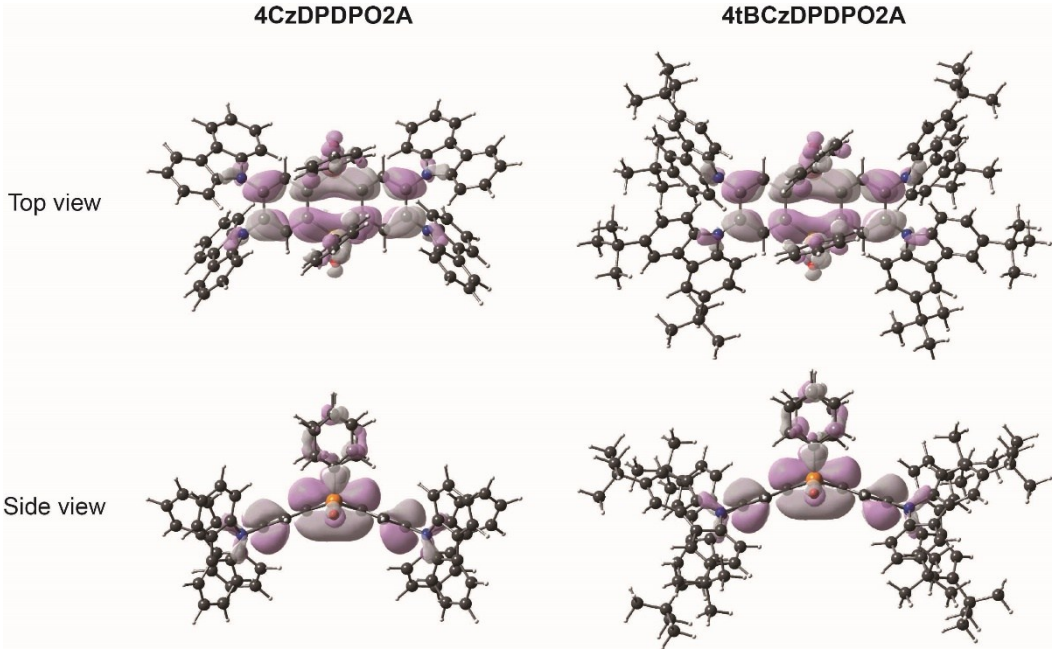

Figure S4. Top and side views of the LUMO contours for **4CzDPDPO2A** and **4tBCzDPDPO2A**.

It is showed that for both **4ArDPDPO2A**, their LUMO orbitals are localized on DPDPO2A acceptors. More importantly, the p-orbitals of sp^2-hybrid C atoms at two sides of P atoms are effectively and directly overlapped without the incorporation of orbitals from P atoms. In this case, it is convincing that DPDPO2A is a homoconjugated unit, since its two phenyls are separated by two continuous C-P single bonds, but directly conjugated through space.

Thermal Properties

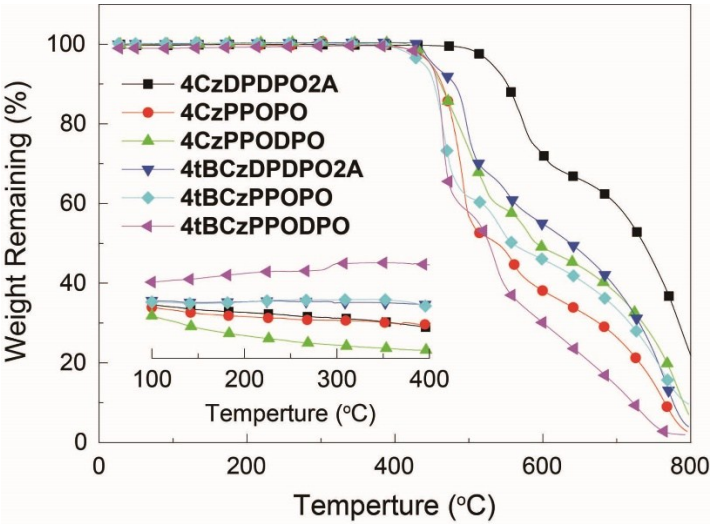

Figure S5. TGA and DSC (inset) curves of **4ArDPDPO2A**, **4ArPPOPO** and **4ArPPODPO**.

Electrochemical Properties

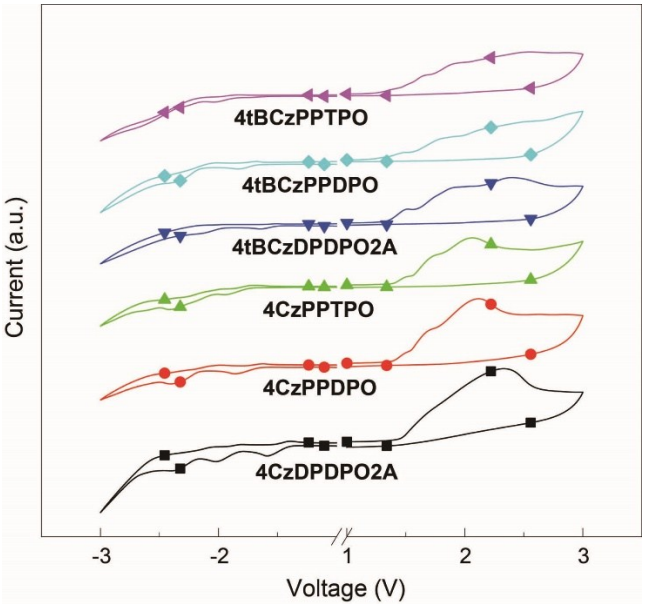

Figure S6. Cyclic voltammograms of **4ArDPDPO2A**, **4ArPPOPO** and **4ArPPODPO** measured at room temperature with a scan rate of 0.1 V s^{-1}.

NTO Analysis Results

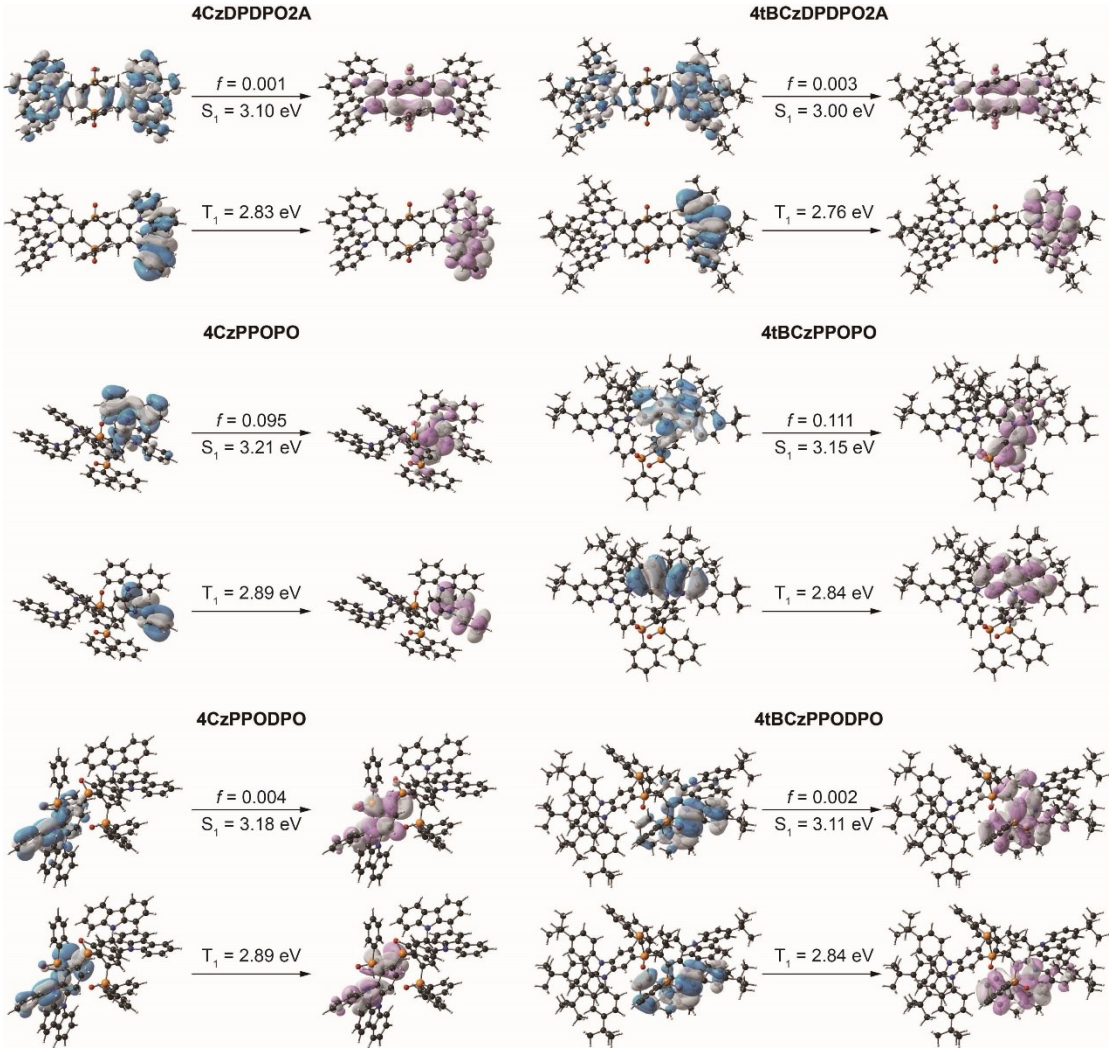

Figure S7. Contours of the HONTOs and LUNTOs and the constants of the $S_0 \rightarrow S_1$ and $S_0 \rightarrow T_1$ excitations for **4ArDPDPO2A**, **4ArPPOPO** and **4ArPPODPO**.

Photophysical Properties

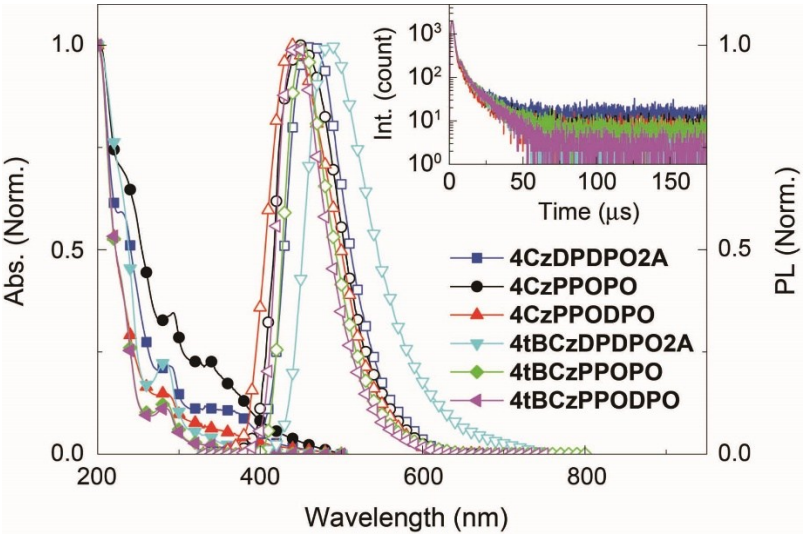

Figure S8. Absorption and steady-state and transient (inset) PL spectra of the vacuum-evaporated films (100 nm) based on neat **4ArDPDPO2A**, **4ArPPOPO** and **4ArPPODPO**.

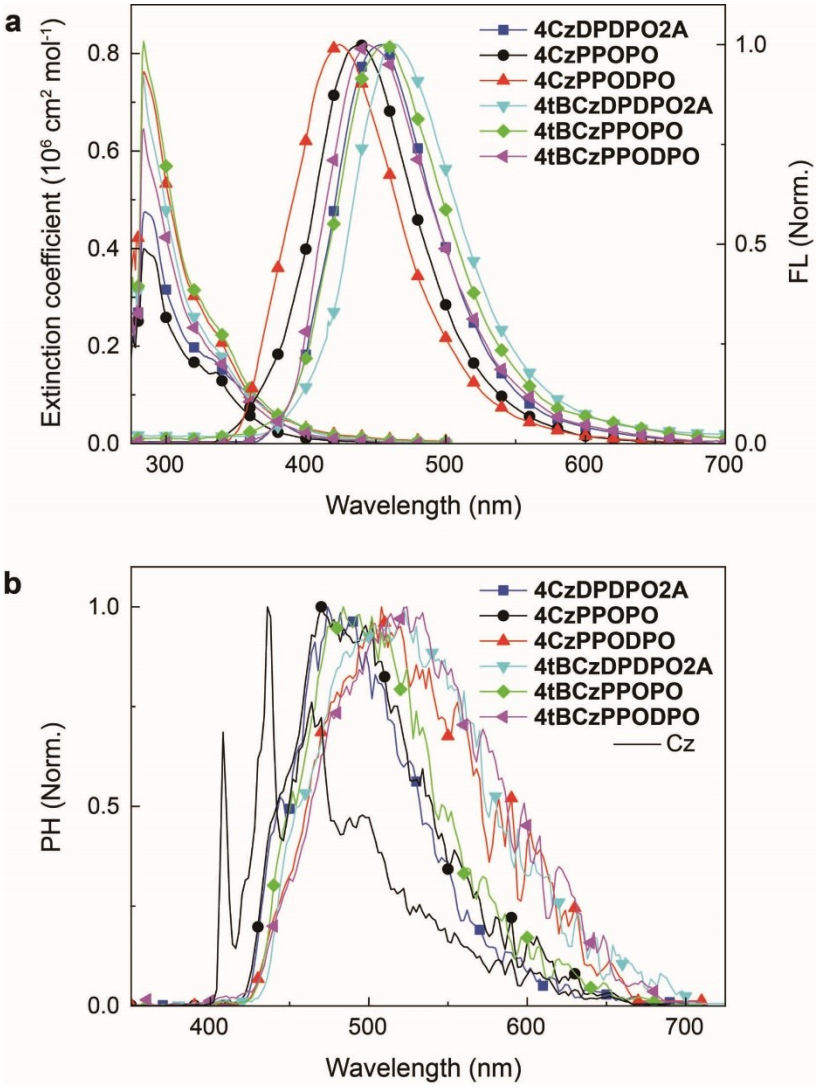

Figure S9. (a) Absorption and fluorescence (FL) and (b) phosphorescence (PH) spectra of **4ArDPDPO2A**, **4ArPPOPO** and **4ArPPODPO**, as well as PH spectrum of carbazole (Cz), in dilute Toluene solutions (10^{-6} mol L^{-1}).

It is showed that due to the intramolecular electronic and vibrational couplings, the 0-0 transitions of PH spectra for **4ArDPDPO2A**, **4ArPPOPO** and **4ArPPODPO** shift red by 30 nm in comparison to that of carbazole (Cz). Nevertheless, the PH spectral regions of these compounds are almost same covering from ~400 to 700 nm. The emissions in the range of 600-700 nm can be attributed to vibrational transitions. The PH emissions of **4ArDPDPO2A**, **4ArPPOPO** and **4ArPPODPO** in this range are stronger than that of Cz, which is due to the degeneracy between different Cz groups and intramolecular coupling in the multi-substituted former.

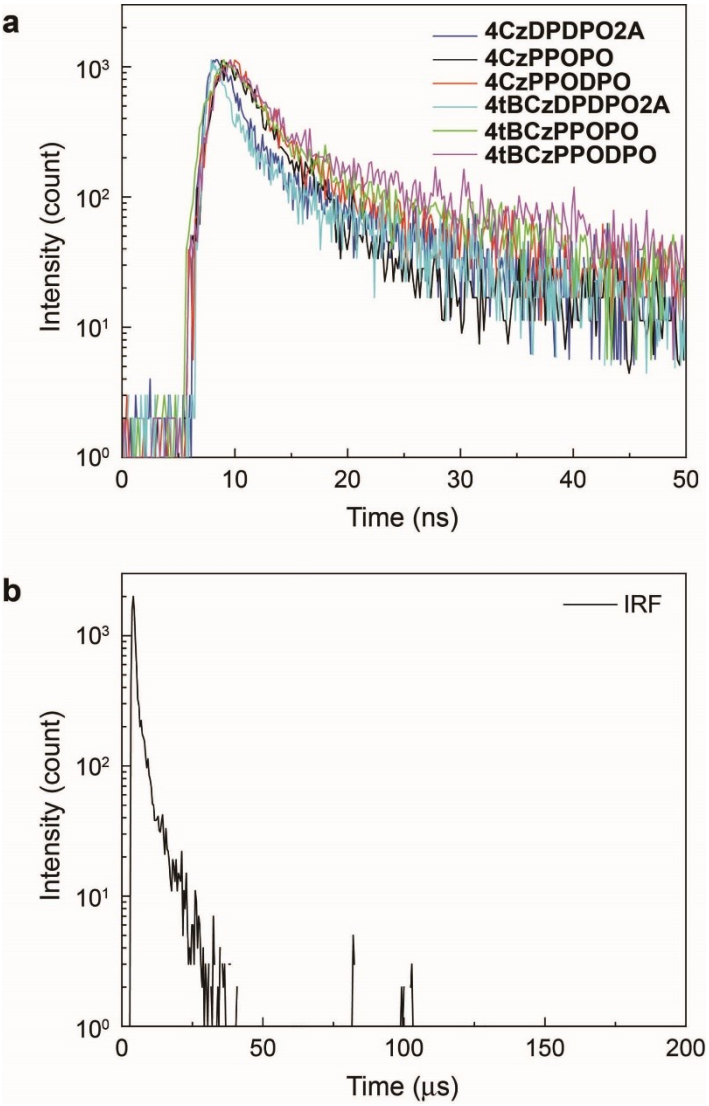

Figure S10. (a) Time decay curves in ns scale of **4ArDPDPO2A**, **4ArPPOPO** and **4ArPPODPO** doped DBFDPO films; (b) Instrumental Response Function (IRF) in μs scale.

It is showed that the PF lifetimes of **4ArDPDPO2A** are remarkably shorter than those of their nonconjugated analogues, accompanied by the higher prompt fluorescence efficiencies for the former. In this case, the shortened prompt fluorescence lifetimes of **4ArDPDPO2A** actually reflect their rapid and efficient singlet radiative transitions, which are facilitated by their more rigid structures and especially the effective frontier molecular orbital overlaps.

AFM Image

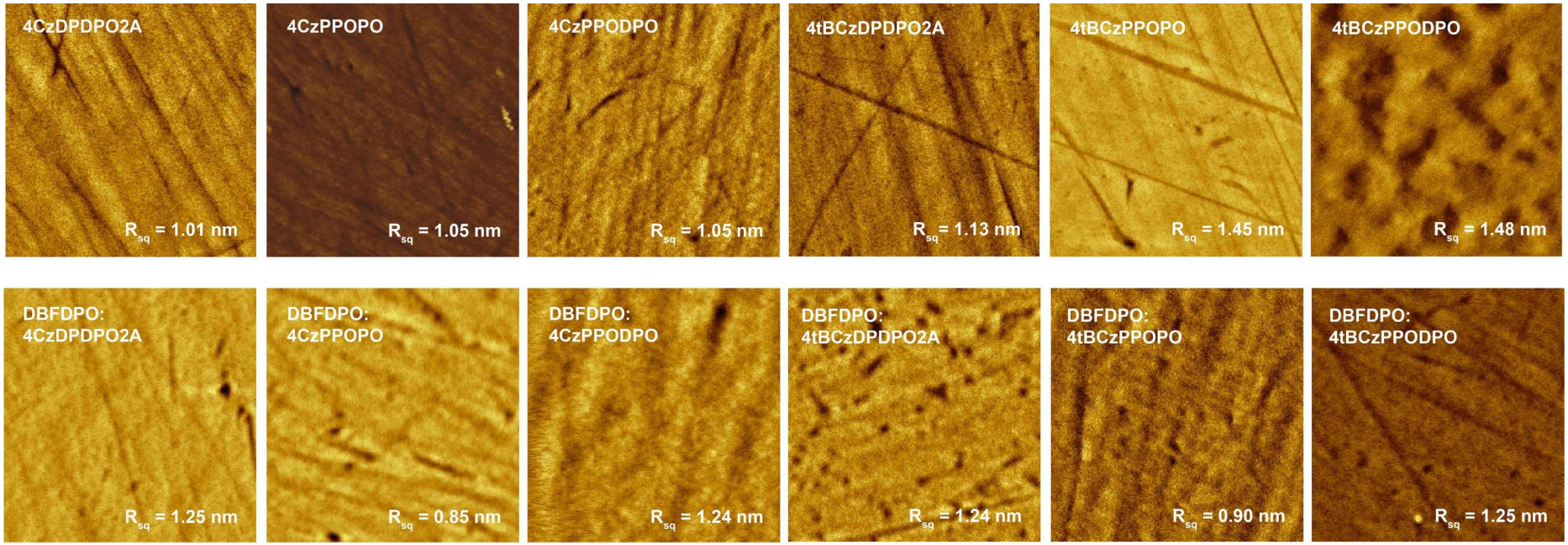

Figure S11. AFM images of the neat and DBFDPO-hosted vacuum-evaporated films (100 nm) for **4ArDPDPO2A**, **4ArPPOPO** and **4ArPPODPO**.

Correlation between Transition Parameters and EQE

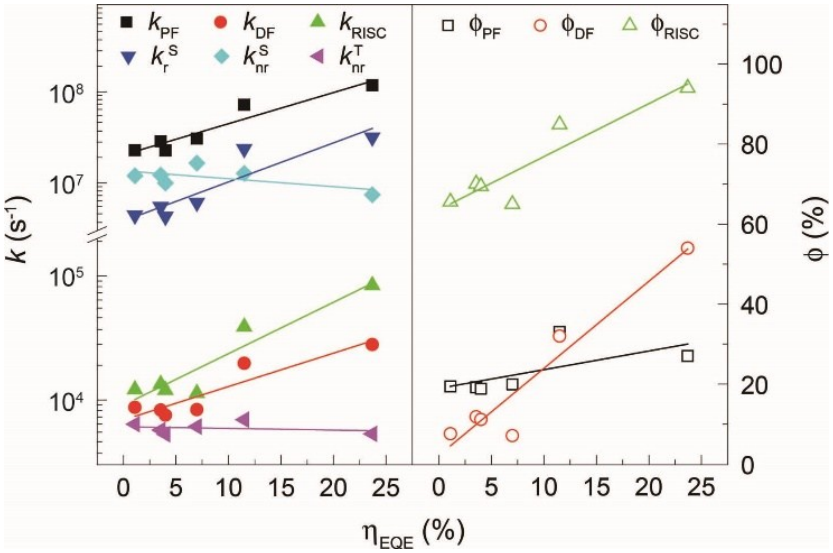

Figure S12. Linear dependence of the maximum ηEQE for the blue OLEDs of **4ArDPDPO2A**, **4ArPPOPO** and **4ArPPODPO** on the rate constant (*k*) and efficiencies (ϕ) of their TADF transitions.

Table S1. DFT and TDDFT results of 4ArDPDPO2A, 4ArPPOPO and 4ArPPODPO.

TADF dye	HOMO (eV)	LUMO (eV)	HOMO-LUMO (eV)	$^0d(\Psi_H-\Psi_L)$[a] (Å)	$^1d(\Psi_H-\Psi_L)$[b] (Å)	$^3d(\Psi_H-\Psi_L)$[c] (Å)	$^0\langle\Psi_H\|\Psi_L\rangle$[d]	$^1\langle\Psi_H\|\Psi_L\rangle$[e]	$^3\langle\Psi_H\|\Psi_L\rangle$[f]	μ_0[g] (Debye)	f_s[h]	S_1 (eV)	T_1 (eV)	ΔE_{ST}[i] (eV)
4CzDPDPO2A	-5.511	-1.911	3.600	2.85	1.68	0.25	0.4300	0.5376	0.8514	5.09	0.0010	3.1	2.83	0.27
4CzPPOPO	-5.356	-1.654	3.702	13.72	7.33	0.29	0.1824	0.4029	0.8557	7.29	0.0951	3.21	2.89	0.32
4CzPPODPO	-5.578	-1.778	3.800	15.24	13.38	0.80	0.0968	0.1695	0.8279	9.03	0.0041	3.18	2.89	0.29
4tBCzDPDPO2A	-5.265	-1.777	3.488	2.80	3.37	0.08	0.4270	0.5134	0.8601	4.45	0.0029	3.00	2.76	0.24
4tBCzPPOPO	-5.130	-1.510	3.620	14.07	7.09	0.21	0.1345	0.4139	0.8521	6.24	0.1106	3.15	2.84	0.31
4tBCzPPODPO	-5.389	-1.624	3.765	15.50	10.19	0.89	0.1036	0.1904	0.8289	7.91	0.0035	3.11	2.84	0.27

[a] Centroid-centroid distance between the HOMO and LUMO; centroid-centroid distances of the [b]singlet and [c]triplet HONTOs and LUNTOs; overlap integrals of [d]the HOMO and LUMO and the [e]singlet and [f]triplet HONTOs and LUNTOs; [g] dipole moments on ground states; [h] oscillator strength of $S_0 \rightarrow S_1$ transition; [i] singlet-triplet splitting.

Table S2. Physical properties of 4ArDPDPO2A, 4ArPPOPO and 4ArPPODPO.

TADF dye	λ_{Abs} (nm)	λ_{PL} (nm)	S_1[c] (eV)	T_1[c] (eV)	ΔE_{ST}[c,d] (eV)	T_d[e] (^oC)	HOMO[f] (eV)	LUMO[f] (eV)	HOMO-LUMO[f] (eV)	μ_e[g] (Debye)
4CzDPDPO2A	228, 285, 334, 357[a] 228, 287, 335, 362[b]	465[a] 467[b]	2.73	2.64	0.09	531	-6.21	-3.38	2.83	8.72
4CzPPOPO	228, 285, 336[a] 228, 293, 338[b]	454[a] 450[b]	2.83	2.62	0.22	448	-6.15	-3.14	3.01	9.16
4CzPPODPO	228, 285, 338[a] 228, 285, 332[b]	436[a] 440[b]	2.92	2.61	0.32	447	-6.16	-3.06	3.10	12.39
4tBCzDPDPO2A	227, 286, 341, 378[a] 228, 283, 336, 374[b]	490[a] 488[b]	2.67	2.62	0.06	452	-6.11	-3.31	2.80	9.48
4tBCzPPOPO	227, 286, 342[a] 228, 288, 326[b]	475[a] 454[b]	2.71	2.58	0.13	439	-6.07	-3.13	2.94	11.11
4tBCzPPODPO	227, 285, 340[a] 228, 284, 337[b]	471[a] 445[b]	2.79	2.56	0.23	448	-6.08	-2.98	3.10	12.16

[a] In chloroform solution (10^{-6} mol L^{-1}); [b] in film; [c] in Toluene solution (10^{-6} mol L^{-1}); [d] singlet-triplet splitting; [e] temperature at weight loss of 5%; [f] calculated according to cyclic voltammetric results; [g] excited-state dipole moment calculated according to Lippert-Mataga relationship.

Table S3. TADF characteristics of 4ArDPDPO2A, 4ArPPOPO and 4ArPPODPO doped DBFDPO films.

TADF dopant	λ_{PL} (nm)	λ_{PH} (nm)	ΔE_{ST} (eV)	ϕ_{PL}[a] (%)	τ_{PF}[b] (ns)	τ_{DF}[c] (μs)	ϕ_{PF}[d] (%)	ϕ_{DF}[e] (%)	k_{PF}[f] (10^7 s^{-1})	k_{DF}[g] (10^4 s^{-1})	k_{ISC}[h] (10^6 s^{-1})	k_{RISC}[i] (10^4 s^{-1})	k_{rj}^S (10^6 s^{-1})	$k_{nr\text{-}k}^S$ (10^6 s^{-1})	$k_{nr\text{-}l}^T$ (10^4 s^{-1})	ϕ_{RISC}[m] (%)
4CzDPDPO2A	470	480	0.05	65	4.6	16.2	33	32	7.17	1.98	35.32	3.89	23.67	12.75	0.69	85
4CzPPOPO	452	468	0.09	27	6.5	8.5	20	7	3.06	0.83	8.05	1.13	6.09	16.48	0.61	65
4CzPPODPO	455	472	0.10	27	8.5	8.7	19	8	2.28	0.87	6.42	1.21	4.44	11.99	0.64	66
4tBCzDPDPO2A	479	484	0.03	81	2.3	19.3	27	54	11.74	2.80	78.26	8.39	31.70	7.43	0.53	94
4tBCzPPOPO	466	474	0.04	31	6.7	14.3	19	12	2.86	0.83	10.92	1.34	5.48	12.20	0.57	70
4tBCzPPODPO	468	476	0.04	30	8.3	14.8	19	11	2.27	0.75	8.44	1.20	4.28	9.98	0.53	69

[a] Absolute PL quantum yield measured with integrating sphere; lifetimes of [b] prompt fluorescence (PF) and [c] delayed fluorescence (DF); efficiencies of [d] PF and [e] DF; rate constants of [f] PF, [g] DF, [h] intersystem crossing (ISC), [i] reverse ISC (RISC), singlet [j] radiation and [k] nonradiation and [l] triplet nonradiation; [m] RISC efficiency.

References

1. Q. Liang, C. Han, C. Duan and H. Xu, *Adv. Opt. Mater.*, 2018, 6, 1800020.
2. A. D. Becke, *J. Chem. Phys.*, 1993, 98, 5648-5652.
3. C. Lee, W. Yang and R. G. Parr, *Phys. Rev. B*, 1988, 37, 785-789.
4. R. L. Martin, *J. Chem. Phys.*, 2003, 118, 4775-4777.
5. M. J. Frisch, G. W. Trucks, H. B. Schlegel, G. E. Scuseria, M. A. Robb, J. R. Cheeseman, G. Scalmani, V. Barone, B. Mennucci, G. A. Petersson, H. Nakatsuji, M. Caricato, X. Li, H. P. Hratchian, A. F. Izmaylov, J. Bloino, G. Zheng, J. L. Sonnenberg, M. Hada, M. Ehara, K. Toyota, R. Fukuda, J. Hasegawa, M. Ishida, T. Nakajima, Y. Honda, O. Kitao, H. Nakai, T. Vreven, J. A. Montgomery, J. E. Peralta, F. Ogliaro, M. Bearpark, J. J. Heyd, E. Brothers, K. N. Kudin, V. N. Staroverov, R. Kobayashi, J. Normand, K. Raghavachari, A. Rendell, J. C. Burant, S. S. Iyengar, J. Tomasi, M. Cossi, N. Rega, J. M. Millam, M. Klene, J. E. Knox, J. B. Cross, V. Bakken, C. Adamo, J. Jaramillo, R. Gomperts, R. E. Stratmann, O. Yazyev, A. J. Austin, R. Cammi, C. Pomelli, J. W. Ochterski, R. L. Martin, K. Morokuma, V. G. Zakrzewski, G. A. Voth, P. Salvador, J. J. Dannenberg, S. Dapprich, A. D. Daniels, Ö. Farkas, J. B. Foresman, J. V. Ortiz, J. Cioslowski and D. J. Fox, Gaussian, Inc., Wallingford CT, USA, D. 1 edn., 2009.